

INSPIRALING DOUBLE COMPACT OBJECT DETECTION AND LENSING RATE – FORECAST FOR DECIGO AND B-DECIGO

ALEKSANDRA PIÓRKOWSKA-KURPAS^{1,2}, SHAOQI HOU³, MAREK BIESIADA^{1,4*}, XUHENG DING^{3,5}, SHUO CAO^{1†}, XILONG FAN³, SEIJI KAWAMURA⁶ AND ZONG-HONG ZHU^{1,3‡}

Draft version March 23, 2022

ABSTRACT

Emergence of gravitational wave (GW) astronomy revived the interest in exploring the low frequency GW spectrum inaccessible from the ground. Satellite GW observatory DECIGO in its original configuration and the currently proposed smaller scale B-DECIGO are aimed to cover deci-Hertz part of the GW spectrum, which fills the gap between LISA mili-Hertz and deca- to kilo-Hertz range probed by ground-based detectors. In this paper we forecast the detection rates of inspiraling double compact objects (DCOs) and the unresolved confusion noise from these sources in DECIGO and B-DECIGO. In the context of DECIGO we use, for the first time, the population synthesis intrinsic inspiral rates of NS-NS, BH-NS and BH-BH systems. We also estimate the expected gravitational lensing rates of such sources for DECIGO and B-DECIGO. The result is that yearly detection of DCOs inspirals for the DECIGO is of order of $10^4 - 10^5$, while for a much smaller scale B-DECIGO they are about $10^2 - 10^4$ depending on the DCO population considered. Taking into account that considerable part of these events would be detectable by ground-based GW observatories the added value of DECIGO/B-DECIGO could be substantial. DECIGO will also be able to register 5 – 50 lensed NS-NS inspirals and up to $O(100)$ BH-BH inspirals. On the contrary, predictions for the B-DECIGO are pessimistic: only the optimistic common envelope scenario of DCO formation could yield a few lensed BH-BH inspirals per year. We also address the question of the magnification bias in the GW event catalogs of DECIGO and B-DECIGO.

Keywords: Gravitational lensing, Gravitational waves: sources

1. INTRODUCTION

First laboratory detections of gravitational waves (GWs) on Earth (Abbott et al. 2016) opened up a new branch of science – GW astronomy. Continuing efforts of LIGO/Virgo team currently conducting the third observational run O3 brought numerous detections of binary black hole (BH-BH) mergers (Abbott et al. 2019a), probably the first mixed black hole - neutron star (BH-NS) merger Abbott et al. (2020) and the first detection of binary neutron star (NS-NS) coalescence (Abbott et al. 2017a). The NS-NS merger was accompanied by identification of its electromagnetic (EM) counterpart and its afterglow was followed up at different EM wavelengths (Goldstein et al. 2017; Coulter et al. 2017). This observation moved multimessenger astronomy to the next level. Besides the tests of general relativity and modified gravity theories (Abbott et al. 2019b), strong bounds on the speed of GWs (Abbott et al. 2017b), GW astronomy has proven that (almost) all classes of double compact objects (DCOs): NS-NS, BH-NS, BH-BH really exist in Nature. The event GW190425 is marginally compatible

with NS-NS merger, so the existence of BH-NS systems still needs to be empirically proven. It is likely that this will happen soon.

Successful operation of ground-based interferometric detectors revived the interest in broadening the GW spectrum to lower frequencies (lower than 1 Hz) fundamentally inaccessible from the ground due to irremovable seismic noise. In particular, LISA was proposed (Amaro-Seoane et al. 2017) as a new generation space mission with a robust strain sensitivity level at frequencies between 0.1 mHz and 100 mHz over a science lifetime of at least 4 years. The technology behind LISA, an ESA-led mission expected to be launched by 2034, has been recently tested by the LISA Pathfinder experiment with outstanding results (Armano et al. 2016). The remaining decihertz band is the target of the DECihertz Interferometer Gravitational wave Observatory (DECIGO), a planned Japanese space-borne GW detector (Kawamura et al. 2019). Original DECIGO (Seto et al. 2001) or currently proposed smaller-scale version B-DECIGO (Sato et al. 2017) are aimed to cover the low-frequency band extending from the mHz to 100 Hz range. DECIGO would be able to detect inspiralling DCO — main targets to LIGO/Virgo, KAGRA or next generation ET, long time (weeks to years) before they enter the hectohertz band accessible from the ground. Moreover, the overlap with ground based GW detectors sensitivity bands is very advantageous since the joint detection with DECIGO and ground based detectors (e.g. ET) would greatly improve the parameter estimation of the binaries.

Reach of the DECIGO will be considerably higher than the next generation of ground based interferomet-

¹ Department of Astronomy, Beijing Normal University, Beijing 100875, China; *caoshuo@bnu.edu.cn; zhuzh@bnu.edu.cn*

² Institute of Physics, University of Silesia, 75 Pułku Piechoty 1, 41-500 Chorzów, Poland

³ School of Physics and Technology, Wuhan University, Wuhan 430072, China

⁴ National Centre for Nuclear Research, Pasteura 7, 02-093 Warsaw, Poland; *Marek.Biesiada@ncbj.gov.pl*

⁵ Department of Physics and Astronomy, University of California, Los Angeles, CA 90095-1547, USA

⁶ Department of Physics, Nagoya University, Nagoya, Aichi 464-8602, Japan

ric detectors, like the ET. With much higher volume probed, one may expect that non-negligible number of GW signals from coalescing DCOs would be gravitationally lensed. Gravitational lensing statistics and magnification cross-sections by galaxies has been discussed e.g. in Zhu & Wu (1997); Zhu (1998). Rates of GW lensing for LIGO/Virgo have been calculated in Ng et al. (2017) and for the ET in Piórkowska et al. (2013); Biesiada et al. (2014); Ding et al. (2015); Li et al. (2018); Oguri (2019); Yang et al. (2019), respectively. The robust prediction is that the third generation of GW interferometric detectors would yield 50 - 100 lensed GW events per year. Strongly lensed GW signals, observed together with their electromagnetic (EM) counterparts, have been demonstrated to enhance our understanding regarding fundamental physics Fan et al. (2017); Collett & Bacon (2017); Cao et al. (2019), dark matter Liao et al. (2018), and cosmology Sereno et al. (2010, 2011); Taylor & Gair (2012); Liao et al. (2017); Wei & Wu (2017). Gravitational lensing of GWs has been widely discussed concerning diffraction effects in lensed GW events Liao et al. (2019); Takahashi & Nakamura (2003); Nakamura (1998), the waveform distortion caused by the gravitational lensing Cao et al. (2014), the influence on the statistical signatures of black hole mergers Dai et al. (2017).

In this paper we make predictions concerning gravitational lensing of GW signals detectable by the DECIGO.

2. GW BACKGROUND NOISE FROM DCO SYSTEMS

We start with the assessment of the background noise created by unresolved DCO systems. In next sections we will discuss the detection rate of such inspiraling systems and their lensing rate by foreground galaxies. In all these considerations one needs the detector’s sensitivity curve and intrinsic DCO merger rates as input. We will discuss these issues below.

2.1. DECIGO sensitivity

DECIGO will be composed of four units of detectors. Each unit is planned to contain three drag-free spacecrafts to form a nearly regular triangle. These four units will be tilted 60° inwards relative to the ecliptic plane to keep its arm lengths nearly constant, and move around the sun with the orbital period of 1 yr. Centers of the triangular configuration of the units will form an equilateral triangle. The fourth one will be anchored to one of the units rotated 180° to form a Star of David configuration. Details concerning the DECIGO design could be found in Yagi & Seto (2011)

For the reference design parameters of DECIGO, one can prove (Yagi & Seto 2011) that a single triangular detector unit is equivalent to two L-shaped interferometers rotated by 45° . Their noises are uncorrelated and the noise spectrum of such an effective L-shaped DECIGO is given by

$$S_h(f) = 10^{-48} \times \left[7.05 \left(1 + \frac{f^2}{f_p^2} \right) + 4.80 \times 10^{-3} \times \frac{f^{-4}}{1 + \left(\frac{f}{f_p} \right)^2} + 5.33 \times 10^{-4} f^{-4} \right] Hz^{-1} \quad (1)$$

where $f_p = 7.36 Hz$.

The original DECIGO mission concept was proposed in 2001 by Seto et al. (2001). What now seems more realistic to be commissioned in the near future is a scaled smaller project called B-DECIGO. It will consist of three satellites in a 100 km equilateral triangle, having sun-synchronous dusk-dawn circular orbits 2000 km above the Earth Sato et al. (2017); Nakamura et al. (2016). With B-DECIGO operating, we will soon probe the decihertz window for the first time, completing the full gravitational spectrum. Therefore we extend our predictions to the B-DECIGO. We use the noise power spectrum density $S_h(f)$ for B-DECIGO proposed by Nakamura et al. (2016); Isoyama et al. (2018)

$$S_h(f) = 10^{-46} \times [4.040 + 6.399 \times 10^{-2} f^{-4} + 6.399 \times 10^{-3} f^2] Hz^{-1} \quad (2)$$

2.2. DCO merger rate from the population synthesis

Previous predictions concerning DECIGO (Yagi & Seto 2011; Yagi 2013) used an analytical approximation of the NS-NS merger rate as a function of redshift up to redshift $z = 5$. Moreover, they did not assess the BH-BH or BH-NS rates precisely. In this paper, we use the values of the intrinsic inspiral rates $\dot{n}_0(z_s)$ forecasted by Dominik et al. (2013) for each type of DCO at redshift slices spanning the range of $z \in [0.04; 17]$. The paper of Dominik et al. (2013) contains the results of detailed population synthesis calculations performed with *StarTrack* evolutionary code (Belczyński et al. 2002). The code is based on well motivated assumptions about star formation rate, galaxy mass distribution, stellar populations, their metallicities and galaxy metallicity evolution with redshift (“low-end” and “high-end” cases), and enables evolving binary systems from ZAMS until the compact binary formation (after supernova explosions). Because the compact object formation depends on the physics of common envelope (CE) phase of evolution and on SN explosion mechanism and both of them are to some degree uncertain, Dominik et al. (2013) considered four scenarios: standard one – based on conservative assumptions and three of its modifications — Optimistic Common Envelope (OCE), delayed SN explosion and high BH kicks scenario. Common envelope phase is a crucial phase of binary evolution from the point of view of DCO formation. The OCE scenario assumes that binaries with Hertzsprung Gap donor stars will lead to DCO formation. Standard scenario makes use of the so called “rapid” convection driven neutrino enhanced SN explosion mechanism. However, if this convection driven neutrino enhanced engine originates from the standing accretion shock instability, the explosion is delayed, which underlies the “delayed SN” scenario. The main effect of this scenario is the modification of DCO mass spectrum. The last issue is that of the natal kicks, which are observationally supported in the case of NS. Natal kicks could be able to disrupt the binary preventing DCO formation. Standard scenario makes a conservative assumption that the velocity of the natal kick is reduced by some factor related to possible fallback of some amount of matter to the newborn compact object. “High BH kicks” scenario assumes that newborn compact object receives the full kick. For more details, see (Dominik et al. 2013) and references therein. We use the data available

at <http://www.syntheticuniverse.org>, more specifically the so called “rest frame rates” in cosmological scenario. For the purpose of our calculations we assume the following values of the chirp masses of DCOs: $1.22 M_\odot$ for NS-NS, $3.2 M_\odot$ for BH-NS and $6.7 M_\odot$ for BH-BH systems. According to Dominik et al. (2012), these values represent average chirp mass for each category of DCO simulated by population synthesis. Moreover, in order to comply with the assumptions underlying population synthesis simulation, we assume flat Λ CDM cosmology with $H_0 = 70 \text{ km s}^{-1} \text{ Mpc}^{-1}$ and $\Omega_m = 0.3$.

2.3. GW background from unresolved DCO systems

Magnitude of a stochastic GW background is usually characterized by its fractional energy density per logarithmic frequency interval

$$\Omega_{GW} = \frac{1}{\rho_{cr}} \frac{d\rho_{GW}}{d \ln f} \quad (3)$$

where $\rho_{cr} = 3H_0^2/8\pi G$ is the critical energy density of the Universe.

According to Phinney (2001) one can conveniently calculate the energy density parameter Ω_{GW}^{DCO} corresponding to the unresolved signals from the DCO systems, as

$$\Omega_{GW}^{DCO} = \frac{8\pi^{5/3}}{9c^2 H_0^2} (GM)^{5/3} f^{2/3} \int_0^\infty \frac{\dot{n}(z)}{(1+z)^{4/3} H(z)} dz \quad (4)$$

where \mathcal{M} is the chirp mass of the DCO system (i.e. NS-NS, BH-NS or BH-BH binary), $\dot{n}(z)$ is the DCO merger rate per proper time per comoving volume at redshift z , and the Hubble parameter $H(z)$ is given by $H(z)^2 = H_0^2[\Omega_m(1+z)^3 + 1 - \Omega_m]$. Calculating numerically the integral in Eq. (4) one obtains

$$\Omega_{GW}^{DCO} = \Omega_0^{DCO} \left(\frac{H_0}{70 \text{ km s}^{-1} \text{ Mpc}^{-1}} \right)^{-3} \times \left(\frac{\mathcal{M}}{\mathcal{M}_{DCO}} \right)^{5/3} \left(\frac{f}{1 \text{ Hz}} \right)^{2/3} \quad (5)$$

where \mathcal{M}_{DCO} is the median value of the DCO considered, i.e. $(\mathcal{M}_{NSNS}; \mathcal{M}_{BHNS}; \mathcal{M}_{BHBH}) = (1.22; 3.2; 6.7) M_\odot$ and values of Ω_0^{DCO} coefficients are reported in Table 1.

In order to compare with the detector’s noise power spectrum the normalized energy density Ω_{GW}^{DCO} should be expressed as the total sky-averaged GW foreground spectrum

$$S_h^{GW,DCO} = \frac{4}{\pi} f^{-3} \rho_{cr} \Omega_{GW}^{DCO} \quad (6)$$

The foreground spectrum of three DCO populations imposed on the DECIGO sensitivity curve is shown in Figure 1. Let us note that B-DECIGO will not be contaminated from the unresolved DCO systems, yet the events like those detected by LIGO/Virgo will be detectable enabling their discovery and study long before they will enter the ground-based detectors sensitivity band.

3. DETECTION RATE FOR UNLENSED EVENTS

Matched filtering signal-to-noise ratio for a single detector reads (Taylor & Gair 2012)

$$\rho = 8\Theta \frac{r_0}{d_L(z_s)} \left(\frac{\mathcal{M}_z}{1.2 M_\odot} \right)^{5/6} \sqrt{\zeta(f_{max})} \quad (7)$$

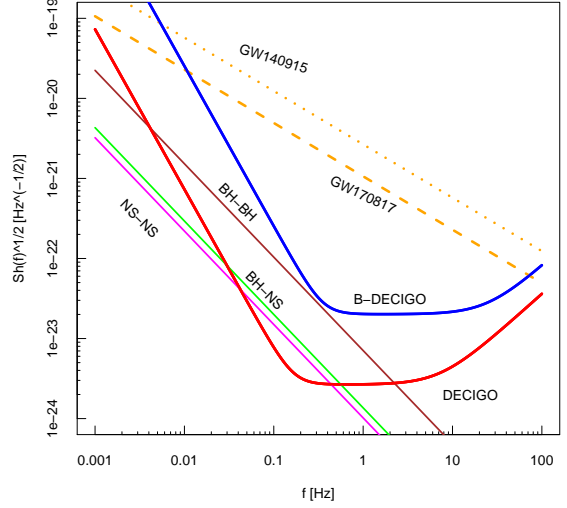


Figure 1. Confusion noise due to DCO systems: NS-NS (magenta), BH-NS (green) and BH-BH (brown) superimposed on the noise spectrum density for DECIGO (red) and B-DECIGO (black). Orange dotted and dashed lines show the effective squared spectrum density corresponding to GW150914 and GW170817 respectively.

where d_L is the luminosity distance to the source, Θ is the orientation factor capturing part of sensitivity pattern due to (usually non-optimal) random relative orientation of DCO system with respect to the detector (more details below). Zeta parameter capturing the overlap between the signal and the detector’s sensitivity band width is defined as

$$\zeta(f_{max}) = \frac{1}{x_{7/3}} \int_0^{2f_{max}} \frac{df (\pi M_\odot)^2}{(\pi f M_\odot)^{7/3} S_h(f)}$$

where $2f_{max}$ is the wave frequency at which the inspiral detection template ends. We assume $\zeta(f_{max}) = 1$, because DCO inspiralling systems studied here will pass the sensitivity band of DECIGO or B-DECIGO. Our assumption is based on actual calculations, which verified it to be true with accuracy of 10^{-4} .

By r_0 we denote the detector’s characteristic distance parameter, which can be estimated according to

$$r_0^2 = \frac{5}{192\pi^{4/3}} \left(\frac{3}{20} \right)^{5/3} \frac{(GM_\odot)^{5/3}}{c^3} f_{7/3}$$

where

$$f_{7/3} = \int_0^\infty [f^{7/3} S_h(f)]^{-1} df$$

Using DECIGO sensitivity Eq. (1) one gets

$$r_0 = 6709 \text{ Mpc.}$$

Similarly, from the B-DECIGO sensitivity given by Eq. (2) one obtains $r_0 = 535 \text{ Mpc.}$, meaning that B-DECIGO will be able to probe about a 1000 times smaller volume than DECIGO.

The orientation factor Θ is defined as

$$\Theta = 2[F_+^2(1 + \cos^2 \iota)^2 + 4F_\times^2 \cos^2 \iota]^{1/2} \quad (8)$$

where $F_+ = \frac{1}{2}(1 + \cos^2 \theta) \cos 2\phi \cos 2\psi - \cos \theta \sin 2\phi \sin 2\psi$ and $F_\times = \frac{1}{2}(1 + \cos^2 \theta) \cos 2\phi \sin 2\psi + \cos \theta \sin 2\phi \cos 2\psi$ are the interferometer strain responses to different polarizations of gravitational wave. The angles (θ, ϕ) describe orientation (polar angles) of direction to the source with respect to the detector plane, (ψ, ι) are the angles describing DCO orbit orientation with respect to the plane tangent to the celestial sphere at source location (so called polarization angle and inclination). The above formulae for $F_{+/\times}$ are for just one L-shaped detector $F_{I;+/\times}$ for the second one it would be $F_{II;+/\times} = F_{I;+/\times}(\theta, \phi - \pi/4, \psi, \iota)$.

Probability distribution for Θ calculated under assumption of uncorrelated orientation angles $(\theta, \phi, \psi, \iota)$ is known to be of the following form

$$P_\Theta(\Theta) = 5\Theta(4 - \Theta)^3/256, \quad \text{if } 0 < \Theta < 4 \quad (9)$$

$$P_\Theta(\Theta) = 0, \quad \text{otherwise}$$

The yearly detection rate of DCO sources originating at redshift z_s and producing the signal with SNR exceeding the detector's threshold $\rho_0 = 8$ (assumption made in previous DECIGO studies (Yagi & Seto 2011; Isoyama et al. 2018)) can be expressed as

$$\dot{N}(> \rho_0 | z_s) = \int_0^{z_s} \frac{d\dot{N}(> \rho_0)}{dz} dz \quad (10)$$

where

$$\frac{d\dot{N}(> \rho_0)}{dz_s} = 4\pi \left(\frac{c}{H_0} \right)^3 \frac{\dot{n}_0(z_s)}{1 + z_s} \frac{\tilde{r}^2(z_s)}{E(z_s)} C_\Theta(x(z_s, \rho_0)) \quad (11)$$

is the rate at which we observe the inspiral DCO events (sources) that originate in the redshift interval $[z, z + dz]$. In Eq. (11) $\dot{n}_0(z_s)$ denotes intrinsic coalescence rate in the local Universe at redshift z_s , $C_\Theta(x) = \int_x^\infty P_\Theta(\Theta) d\Theta$

$$\text{and } x(z, \rho) = \frac{\rho}{8} (1 + z)^{1/6} \frac{c}{H_0} \frac{\tilde{r}(z)}{r_0} \left(\frac{1.2 M_\odot}{\mathcal{M}_0} \right)^{5/6}.$$

Here, and throughout this paper we use the values of inspiral rates $\dot{n}_0(z_s)$ obtained with **StarTrack** evolutionary code. The results are summarized in Table 2. Probability density of DCO inspiral events as a function of redshift is shown in Fig 2. Similar predictions for the B-DECIGO are given in Table 3. One can see that even though B-DECIGO is considerably smaller scale enterprise, it would be able to register hundreds of NS-NS inspirals and thousands of BH-BH inspirals per year.

4. LENSED GW SIGNALS STATISTICS

Concerning gravitational lensing we adopt the same approach as in our previous papers (Piórkowska et al. 2013; Biesiada et al. 2014; Ding et al. 2015), i.e. we assume conservatively that the population of lenses comprise only elliptical galaxies. Therefore, we will model the lenses as singular isothermal spheres (SIS) which is a good approximation of early type galaxies (Koopmans et al. 2009). Characteristic angular scale of lensing phenomenon is set by the Einstein radius, which for the SIS model reads $\theta_E = 4\pi \left(\frac{\sigma}{c} \right)^2 \frac{d_A(z_l, z_s)}{d_A(z_s)}$, where σ is the velocity dispersion of stars in lensing galaxy, $d_A(z_l, z_s)$ and $d_A(z_s)$ are angular diameter distances between the lens and the source and to the source, respectively (Cao et

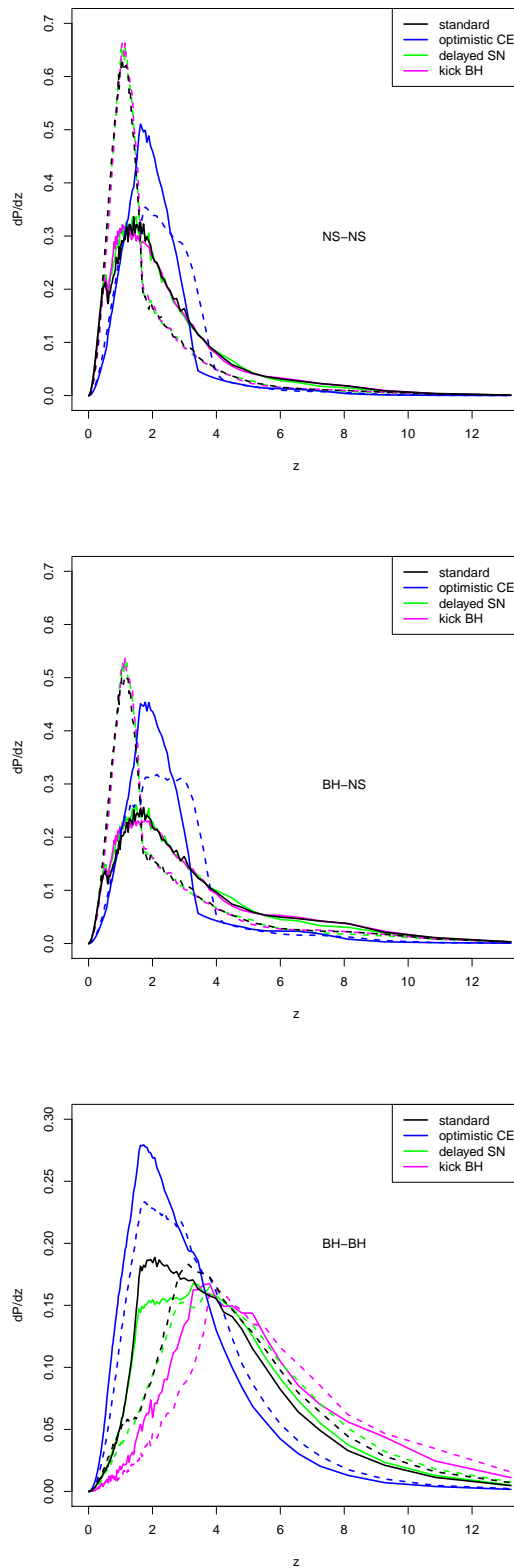


Figure 2. Probability density of DCO inspiral events as a function of redshift for the DECIGO. Different colors refer to different scenarios: black – standard, blue – OCE, green – delayed SN, magenta – high BH kicks. Solid line corresponds to the low-end metallicity evolution, dashed line – high-end metallicity.

Table 1
Numerical factors Ω_0^{DCO} in the Eq. (5) for different classes of DCO systems under different evolutionary scenarios, assuming “low-end” and “high-end” metallicity evolution.

Evolutionary scenario	$\Omega_0^{DCO} \times 10^{-12}$			
	standard	optimistic	delayed SN	high BH kicks
NS-NS				
low-end metallicity	1.33	10.26	1.51	1.34
high-end metallicity	2.17	9.95	2.44	2.14
BH-NS				
low-end metallicity	2.37	6.43	1.28	2.34
high-end metallicity	1.40	4.89	0.76	0.16
BH-BH				
low-end metallicity	63.90	343.69	49.29	2.41
high-end metallicity	42.48	233.44	30.23	1.57

Table 2
Yearly detection rate of inspiralling DCOs of different classes under different evolutionary scenarios, assuming “low-end” and “high-end” metallicity evolution. Predictions for the DECIGO.

Yearly detection rate	standard	optimistic CE	delayed SN	high BH kicks
$\dot{N}(> \rho_0)$ [yr^{-1}] for NS-NS				
low-end metallicity	27573.2	326220.6	30469.4	28036.9
high-end metallicity	40514.7	309561.2	45400.9	42034.9
$\dot{N}(> \rho_0)$ [yr^{-1}] for BH-NS				
low-end metallicity	25629.6	49393.8	13072.0	2673.7
high-end metallicity	18534.5	43165.3	9719.3	2155.7
$\dot{N}(> \rho_0)$ [yr^{-1}] for BH-BH				
low-end metallicity	353305.4	1137125.0	286116.6	20840.9
high-end metallicity	263272.6	955313.4	212626.4	15561.3
$\dot{N}(> \rho_0)$ [yr^{-1}] for total				
low-end metallicity	406508.2	1512739.4	329658.0	51551.5
high-end metallicity	322321.8	1308039.9	267746.6	59751.9

Table 3
Yearly detection rate of inspiralling DCOs of different classes under different evolutionary scenarios, assuming “low-end” and “high-end” metallicity evolution. Predictions for B-DECIGO.

Yearly detection rate	standard	optimistic CE	delayed SN	high BH kicks
$\dot{N}(> \rho_0)$ [yr^{-1}] for NS-NS				
low-end metallicity	136.4	394.4	154.3	129.4
high-end metallicity	159.1	448.7	179.2	147.6
$\dot{N}(> \rho_0)$ [yr^{-1}] for BH-NS				
low-end metallicity	183.5	801.5	119.0	17.0
high-end metallicity	102.6	572.9	54.0	8.9
$\dot{N}(> \rho_0)$ [yr^{-1}] for BH-BH				
low-end metallicity	9473.2	76548.7	7236.5	192.3
high-end metallicity	5476.7	46748.3	3485.2	100.7
$\dot{N}(> \rho_0)$ [yr^{-1}] for total				
low-end metallicity	9793.1	77780.6	7509.8	338.7
high-end metallicity	5738.4	47769.9	3718.4	257.2

al. 2012, 2015). It is convenient to use the Einstein radius as a unit and convert the angular distance of the image (w.r.t. the center of the lens) θ or the angular position of the source β to respective dimensionless parameters $x = \frac{\theta}{\theta_E}$, $y = \frac{\beta}{\theta_E}$. Then the necessary condition for strong lensing (appearance of multiple images) is $y < 1$. Images (brighter I_+ and fainter one I_-) form at locations $x_{\pm} = 1 \pm y$ with magnifications $\mu_{\pm} = \frac{1}{y} \pm 1$.

Hence, the gravitationally lensed GW signal would come from these two images with appropriate relative time delay $\Delta t = \Delta t_0(\sigma, z_l, z_s)y$ (for details see (Piórkowska et al. 2013; Biesiada et al. 2014)) and with different amplitudes $h_{\pm} = \sqrt{\mu_{\pm}} h(t) = \sqrt{\frac{1}{y} \pm 1} h(t)$ where $h(t)$ denotes the intrinsic amplitude (i.e. the one which would have been observed without lensing). Analogous relations are valid for the SNR parameter ρ . Assuming the threshold SNR

for detection $\rho_0 = 8$, one can observe lensed images (of the source with an intrinsic SNR equal to $\rho_{intr.}$) if the misalignment of the source with respect to the optical axis of the lens satisfies

$$y_{\pm} \leq y_{\pm, max} = \left[\left(\frac{8}{\rho_{intr.}} \right)^2 \mp 1 \right]^{-1} \quad (12)$$

The condition of $\rho > 8$ for the I_+ and I_- image separately influence the elementary cross section for lensing (see e.g. (Piórkowska et al. 2013))

$$\begin{aligned} S_{cr, \pm}(\sigma, z_l, z_s, \rho) &= \pi \theta_E^2 y_{\pm, max}^2 \\ &= 16\pi^3 \left(\frac{\sigma}{c} \right)^4 \left(\frac{\tilde{r}_{ls}}{\tilde{r}_s} \right)^2 y_{\pm, max}^2 \end{aligned} \quad (13)$$

which is necessary to calculate optical depth for lensing leading to magnifications of I_+ and I_- images above the threshold

$$\begin{aligned} \tau_{\pm}(z_s, \rho) &= \frac{1}{4\pi} \int_0^{z_s} dz_l \int_0^{\infty} d\sigma 4\pi \left(\frac{c}{H_0} \right)^3 \times \\ &\quad \frac{\tilde{r}_l^2}{E(z_l)} S_{cr, \pm}(\sigma, z_l, z_s) \frac{dn}{d\sigma} \end{aligned} \quad (14)$$

In analogy to our previous papers, (Piórkowska et al. 2013; Biesiada et al. 2014; Ding et al. 2015), we model the velocity dispersion distribution in the population of lensing galaxies as a modified Schechter function $\frac{dn}{d\sigma} = n_* \left(\frac{\sigma}{\sigma_*} \right)^{\alpha} \exp \left(- \left(\frac{\sigma}{\sigma_*} \right)^{\beta} \right) \frac{\beta}{\Gamma(\frac{\alpha}{\beta})} \frac{1}{\sigma}$ with parameters n_*, σ_*, α and β taken after Choi, Park & Vogelej (2007). The choice of this particular model, despite the existence of more recent data on velocity dispersion distribution functions is motivated by its best representing the pure elliptical galaxy population in agreement with our model assumption (Biesiada et al. 2014).

In order to confirm the detection of a lensed GW source the fainter image should have SNR higher than threshold, so the misalignment must not exceed the limiting value given by Eq. (12). This influences the elementary cross-section Eq. (13) and further propagates into formulae for optical depth for lensing. In particular differential (with respect to the lens redshift) optical depth for lensing reads

$$\frac{d\tau_{\pm}}{dz_l} = 16\pi^3 \left(\frac{c}{H_0} \right)^3 \frac{\tilde{r}_{ls}^2 \tilde{r}_l^2}{\tilde{r}_s^2 E(z_l)} y_{\pm, max}^2 n_* \left(\frac{\sigma_*}{c} \right)^4 \frac{\Gamma \left(\frac{4+\alpha}{\beta} \right)}{\Gamma \left(\frac{\alpha}{\beta} \right)} \quad (15)$$

and the total optical depth is

$$\tau_{\pm} = \frac{16}{30} \pi^3 \left(\frac{c}{H_0} \right)^3 \tilde{r}_s^3 \left(\frac{\sigma_*}{c} \right)^4 n_* \frac{\Gamma \left(\frac{4+\alpha}{\beta} \right)}{\Gamma \left(\frac{\alpha}{\beta} \right)} y_{\pm, max}^2 \quad (16)$$

The above formulae are valid only in the case of a continuous search. If instead the survey has a finite duration T_{surv} some of the events, i.e. those whose signals come near the beginning or the end of the survey, would be lost because of lensing time delay. In other words we would register the signal from just one image and cannot tell

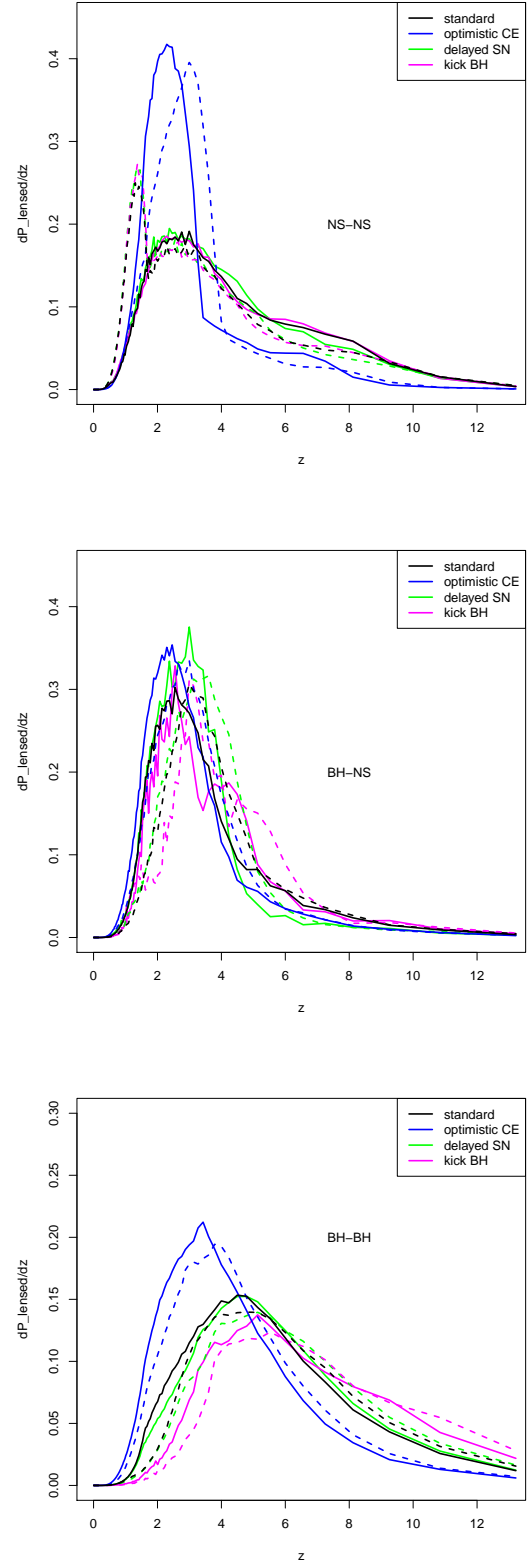


Figure 3. Differential lensing rate $\frac{1}{N^{lensed}} \frac{d\dot{N}^{lensed}}{dz}$ (as a function of source redshift) of DCO inspiralling binaries for two different evolutionary scenarios. Black line is for the standard scenario, blue one – for the optimistic CE. Low-end metallicity evolution scenario assumed. Predictions for the DECIGO.

Table 4

Expected numbers of lensed GW events from inspiralling DCOs of different classes under different evolutionary scenarios, assuming “low-end” and “high-end” metallicity evolution. Predictions for the DECIGO.

Evolutionary scenario T_{surv}	standard (1yr; 4yrs;10yrs)	optimistic CE (1yr; 4yrs;10yrs)	delayed SN (1yr; 4yrs;continuous)	high BH kicks (1yr; 4yrs;10yrs)
NS-NS				
low-end metallicity	(5.2; 6.1; 6.3)	(46.8; 53.4; 54.7)	(5.5; 6.4; 6.6)	(5.2; 6.1; 6.3)
high-end metallicity	(5.2; 6.0; 6.2)	(49.5; 56.7; 58.2)	(5.7; 6.5; 6.7)	(5.4; 6.2; 6.4)
BH-NS				
low-end metallicity	(4.8; 5.5; 5.7)	(7.4; 8.5; 8.7)	(2.3; 2.6; 2.7)	(0.6; 0.6; 0.7)
high-end metallicity	(4.3; 5.0; 5.1)	(7.7; 8.8; 9.0)	(2.1; 2.4; 2.5)	(0.5; 0.6; 0.6)
BH-BH				
low-end metallicity	(114.5; 136.1; 140.5)	(261.1; 305.4; 314.2)	(97.5; 116.2; 119.9)	(8.7; 10.5; 10.8)
high-end metallicity	(97.1; 116.1; 119.9)	(249.1; 292.9; 301.7)	(81.9; 98.2; 101.5)	(7.1; 8.6; 8.9)
TOTAL				
low-end metallicity	(130.1; 156.2; 162.7)	(325.7; 383.3; 397.7)	(110.2; 132.7; 138.3)	(15.0; 18.0; 18.8)
high-end metallicity	(111.7; 134.8; 140.6)	(316.9; 374.8; 389.2)	(94.2; 113.9; 118.8)	(13.4; 16.1; 16.7)

Table 5

Expected numbers of lensed GW events from inspiralling DCOs of different classes under different evolutionary scenarios, assuming “low-end” and “high-end” metallicity evolution. Predictions for the B-DECIGO.

Evolutionary scenario T_{surv}	standard 4yrs	optimistic CE 4yrs	delayed SN 4yrs	high BH kicks 4yrs
NS-NS				
low-end metallicity	0.0001	0.0004	0.0001	0.0001
high-end metallicity	0.0002	0.0004	0.0002	0.0001
BH-NS				
low-end metallicity	0.002	0.01	0.001	0.0001
high-end metallicity	0.001	0.01	0.001	0.0001
BH-BH				
low-end metallicity	0.6	3.7	0.4	0.01
high-end metallicity	0.3	2.5	0.2	0.01

that in fact the event was lensed. Such a case can be handled by a proper correction to (15) or (14), e.g.,

$$\tau_{\Delta t, \pm} = \tau \left[1 - \frac{1}{7} \frac{\Gamma\left(\frac{\alpha+8}{\beta}\right)}{\Gamma\left(\frac{\alpha+4}{\beta}\right)} \frac{\Delta t_{*, \pm}}{T_{surv}} \right] \quad (17)$$

where $\Delta t_{*, \pm} = \frac{32\pi^2}{H_0} \tilde{r}_s \left(\frac{\sigma_*}{c}\right)^4 y_{\pm, max}$ (for detailed calculations see Piórkowska et al. (2013)). These corrections are particularly important because the DECIGO and B-DECIGO missions are planned for $T_{surv} = 4$ yr. We present predictions for the first year of operation and for the total 4 yrs of nominal duration. However, like LISA, the DECIGO could finally be designed with consumables and orbital stability to facilitate mission up to 10 yrs in duration. Therefore, we report the predictions for $T_{surv} = 10$ yr as well.

We start with a conservative assumption that the lensed system is intrinsically loud enough to exceed the detector’s threshold $\rho_0 = 8$. and we assume that the fainter image exceeds the threshold. This means that we only consider $y_{max} = y_{-, max} = 0.5$, according to Eq. (12).

Cumulative yearly detection of lensed events up to the

source redshift z_s can be calculated as

$$\dot{N}_{lensed}(z_s) = \int_0^{z_s} \tau_{\Delta t}(z_s, y_{max}, T_{surv}) \frac{d\dot{N}(> \rho_0)}{dz} dz \quad (18)$$

The results are shown in Table 4. In Fig. 3 normalized differential lensing rate (as a function of redshift) is displayed. One can see that DECIGO in its original design would be able to register 5–6 strongly lensed NS-NS (or BH-NS) systems, which could be accompanied by the EM counterpart during their final merger phase detectable by ground based interferometric detectors. These are the most promising lensed sources enabling e.g precise cosmological inference (Liao et al. 2017) or probing dark matter substructure in lensing galaxies (Liao et al. 2018). Much more, i.e. about 100 lensed inspirals could be seen from the BH-BH binary systems. On the other hand lensing statistics forecasts for the DECIGO are very pessimistic – only within the optimistic CE scenario of DCO formation one could have hope of registering a few lensed BH-BH inspirals.

5. CONCLUSIONS

In this paper we have made the predictions of yearly detection rates of GW signals from the DCO inspirals detectable in the future decihertz space-borne detectors DECIGO and its smaller scale version B-DECIGO. All previous papers concerning DECIGO used only analyt-

ical estimates of NS-NS merger rates up to $z = 5$. In our calculations, we have used for the first time the **StarTrack** population synthesis results concerning intrinsic merger rates at different redshifts of distinct classes of DCO systems: NS-NS, BH-NS and BH-BH binaries. We have also estimated the stochastic noise levels due to unresolved DCO systems. The conclusion is that DECIGO would be significantly contaminated by BH-BH binary systems, while the level of this stochastic noise component is not relevant for B-DECIGO. Concerning the DCO yearly detection rate its order of magnitude ranges from 10^4 for NS-NS and BH-NS systems to 10^5 for BH-BH systems in DECIGO. Respective rates for the B-DECIGO are 10^2 (NS-NS or BH-NS) and 10^3 (BH-BH).

The detector's distance parameter r_0 for the DECIGO is about 4 times bigger than for the ET, meaning that DECIGO will probe 64 times bigger volume than the next generation of ground based detectors. Hence, we addressed the issue of gravitationally lensed DCO inspirals observable by the DECIGO. For the completeness of discussion we considered B-DECIGO as well, even though B-DECIGO's r_0 is about 3 times smaller than for the ET. Our basic assessment was performed under assumption that the GW source is intrinsically loud (i.e. would be detectable without lensing). The result is that DECIGO will also be able to register 5 – 50 lensed NS-NS inspirals and up to $O(100)$ BH-BH inspirals. On the contrary, predictions for the B-DECIGO are pessimistic: only the optimistic common envelope scenario of DCO formation could result with a few of lensed BH-BH inspirals per year. In the appendix we enrich our discussion relaxing the $\rho_{intr.} \geq 8$ assumption and consider intrinsically faint signals, i.e. those being detectable exclusively due to lensing magnification. Such inclusion of lensing magnification would significantly enlarge the statistics of lensed events with intrinsic SNR $\rho_{intr.} \geq 8$ for both DECIGO and B-DECIGO. The appendix also addresses the question of the magnification bias in the full inspiral GW event catalogs of DECIGO and B-DECIGO. One finds out that the magnification bias is of the order of $10^{-3} - 10^{-4}$, which means that the cosmological inferences drawn from these catalogs would not be affected very much.

Let us stress that DECIGO and B-DECIGO would be able to register inspiral signals from the DCOs years before they enter the high frequency band of ground-based detectors to finally end their lives in energetic mergers. Having in mind this circumstance and the benefits that are expected from registering lensed GW (especially those accompanied by the EM signals) one would expect that DECIGO's detections of lensed GW signals could trigger a concerted efforts for searching strong lenses in the EM domain at possible locations suggested by the DECIGO. This would be very profitable in many aspects, in particular for identifying the host galaxy before the merger and despite of no bright EM counterpart as it was the case to the BH-BH mergers registered so far. However, unlike the ground-based detector where one registers a transient event, DECIGO would observe lensed events in an adiabatic inspiral phase as two (or more) unresolved images, likely producing interference patterns in the waveforms. This is besides the scope of the present paper which focused only on the statistics of

GW lensing and will be the subject of a separate study.

ACKNOWLEDGMENTS

This work was supported by National Key R&D Program of China No. 2017YFA0402600; the National Natural Science Foundation of China under Grants Nos. 11690023, 11373014, and 11633001; Beijing Talents Fund of Organization Department of Beijing Municipal Committee of the CPC; the Strategic Priority Research Program of the Chinese Academy of Sciences, Grant No. XDB23000000; the Interdiscipline Research Funds of Beijing Normal University; and the Opening Project of Key Laboratory of Computational Astrophysics, National Astronomical Observatories, Chinese Academy of Sciences. This work was initiated at Aspen Center for Physics, which is supported by National Science Foundation grant PHY-1607611. This work was partially supported by a grant from the Simons Foundation. M.B. is grateful for this support.

APPENDIX - LENSING OF INTRINSICALLY FAINT GW SOURCES

Gravitational lensing magnifies the lensed images of the source. Therefore, one can relax the assumption that sources should be intrinsically loud enough to be detected without lensing and treat their signal to noise parameter ρ as a free one. In such a case one would get estimates for the population of DCO systems detectable exclusively due to gravitational lensing. In other words this would provide forecasts for magnification bias in the catalog of lensed DCO inspirals. We will follow the strategy used in Ding et al. (2015) in the case of the ET. Therefore, instead of Eq. (11) we have to start with the differential inspiral rate per redshift and per SNR parameter ρ

$$\frac{\partial^2 \dot{N}}{\partial z_s \partial \rho} = 4\pi \left(\frac{c}{H_0} \right)^3 \frac{\dot{n}_0(z_s) \tilde{r}^2(z_s)}{1 + z_s E(z_s)} P_{\Theta}(x(z_s, \rho)) \frac{x(z_s, \rho)}{\rho} \quad (19)$$

then one should calculate cross-sections $S_{cr, \pm}$ and optical depths τ_{\pm} for lensing separately for each image I_+ or I_- . The final result will be the lensing rate of intrinsically faint ($\rho < \rho_0$) DCOs having I_+ or I_- images magnified above the threshold ρ_0

$$\dot{N}_{lensed, \pm} = \int_0^{z_{max}} dz_s \int_0^{\rho_0} \tau_{\Delta t, \pm}(z_s, \rho) \frac{\partial^2 \dot{N}}{\partial z_s \partial \rho} d\rho \quad (20)$$

or differential lensing rates with respect to ρ or z_s respectively

$$\frac{d\dot{N}_{lensed, \pm}}{d\rho} = \int_0^{z_{max}} \tau_{\Delta t, \pm}(z_s, \rho) \frac{\partial^2 \dot{N}}{\partial z_s \partial \rho} dz_s \quad (21)$$

$$\frac{d\dot{N}_{lensed, \pm}}{dz_s} = \int_0^{\rho_0} \tau_{\Delta t, \pm}(z_s, \rho) \frac{\partial^2 \dot{N}}{\partial z_s \partial \rho} d\rho \quad (22)$$

Table 6 contains the results of predicted intrinsically faint lensed GW events for which the the I_- image is magnified above threshold $\rho_0 = 8$ for DECIGO, and Table 7 is for B-DECIGO. As one can see, inclusion of lensing magnification of intrinsically faint events would significantly enlarge the statistics of lensed events with intrinsic SNR $\rho_{intr} \geq 8$ (see Tab. 4 and Tab. 5). This conclusion is true both for DECIGO and B-DECIGO.

Table 6

Expected numbers of lensed GW events observed by DECIGO with $\rho_{intr} < 8$ for which the I_- image is magnified above threshold $\rho_0 = 8$. We also assumed the continuous survey, which in practice means that its duration is longer than 5 years. Nomenclature of DCO formation scenarios and galaxy metallicity evolution follows that of Dominik et al. (2013).

Evolutionary scenario T_{surv}	standard (4yrs;continuous)	optimistic CE (4yrs;continuous)	delayed SN (4yrs;continuous)	high BH kicks (4yrs;continuous)
NS-NS				
low-end metallicity	(3.5;3.6)	(18.8;19.5)	(3.5;3.7)	(3.5;3.6)
high-end metallicity	(3.1;3.3)	(21.3;22.1)	(3.3;3.4)	(3.2;3.3)
BH-NS				
low-end metallicity	(0.4;0.4)	(0.6;0.6)	(0.2;0.2)	(0.05;0.05)
high-end metallicity	(0.4;0.4)	(0.6;0.7)	(0.2;0.2)	(0.05;0.06)
BH-BH				
low-end metallicity	(4.6;4.9)	(8.6;8.9)	(4.1;4.3)	(0.4;0.4)
high-end metallicity	(4.2;4.4)	(8.8;9.1)	(3.7;3.9)	(0.4;0.4)
TOTAL				
low-end metallicity	(8.5;8.9)	(28.0;29.0)	(7.8;8.2)	(3.6;4.1)
high-end metallicity	(7.7;8.1)	(30.7;31.9)	(7.3;7.5)	(3.7;3.8)

Table 7

Expected numbers of lensed GW events observed by B-DECIGO with $\rho_{intr} < 8$ for which the I_- image is magnified above threshold $\rho_0 = 8$. We also assumed the continuous survey, which in practice means that its duration is longer than 5 years. Nomenclature of DCO formation scenarios and galaxy metallicity evolution follows that of Dominik et al. (2013).

Evolutionary scenario T_{surv}	standard (4yrs;10yrs)	optimistic CE (4yrs;10yrs)	delayed SN (4yrs;10yrs)	high BH kicks (4yrs;10yrs)
NS-NS				
low-end metallicity	(0.01;0.01)	(0.1;0.2)	(0.01;0.01)	(0.01;0.01)
high-end metallicity	(0.02;0.02)	(0.1;0.1)	(0.02;0.02)	(0.02;0.02)
BH-NS				
low-end metallicity	(0.1;0.1)	(0.2;0.3)	(0.07;0.07)	(0.01;0.01)
high-end metallicity	(0.9;0.9)	(0.2;0.2)	(0.05;0.05)	(0.01;0.01)
BH-BH				
low-end metallicity	(9.0;9.1)	(28.3;28.9)	(7.2;7.3)	(0.5;0.5)
high-end metallicity	(6.5;6.7)	(24.3;24.8)	(5.2;5.3)	(0.4;0.4)
TOTAL				
low-end metallicity	(9.1;9.2)	(28.6;29.4)	(7.3;7.4)	(0.5;0.5)
high-end metallicity	(7.4;7.6)	(24.6;25.1)	(5.3;5.4)	(0.4;0.4)

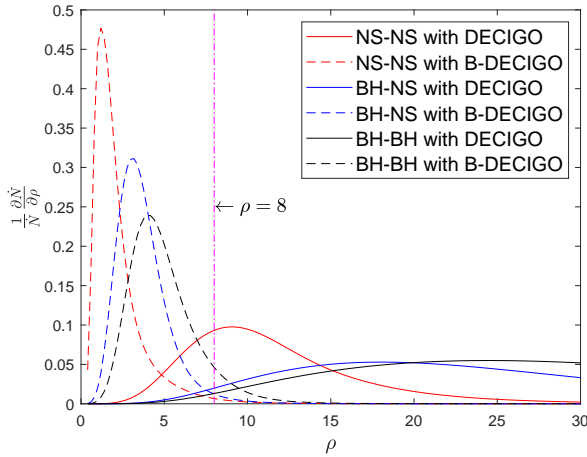


Figure 4. The normalized differential yearly detection rates $\frac{1}{N} \frac{\partial \dot{N}}{\partial \rho}$ v.s. the intrinsic SNR ρ . “Low-end” metallicity galaxy evolution and the standard model of DCO formation are assumed.

The normalized differential yearly detection rates $\frac{1}{N} \frac{\partial \dot{N}}{\partial \rho}$ of lensed events as functions of the intrinsic SNR

ρ for various types of DCOs to be observed by DECIGO and B-DECIGO are displayed in Fig. 4.

Figure 5 shows the normalized differential yearly detection rates $\frac{1}{N} \frac{\partial \dot{N}}{\partial z_s}$ of lensed events as functions of the source redshift z_s . The top panel illustrates lensed faint systems with $\rho_{intr} < 8$ with the I_- image magnified above the threshold. In other words, both images will be registered by DECIGO or B-DECIGO. In the lower panel differential detection rate is shown for systems of both $\rho_{intr} < 8$ and $\rho_{intr} \geq 8$, i.e. for the total catalog of lensed GW events of DECIGO or B-DECIGO. For the sake of transparency only standard scenario of DCO formation with “low-end” metallicity evolution is shown. Detector’s operation period of $T_{surv} = 4$ years is assumed. From these figures, one infers that the faint sources can be used to probe higher redshifts, and these higher redshift sources would thus contaminate the future catalog of gravitationally lensed GW events. This is expected on the ground of general idea of how the magnification bias works. Since DECIGO’s characteristic radius r_0 is much larger than that of B-DECIGO, the former configuration is more suitable to probe high

redshift sources, as shown by Fig. 5.

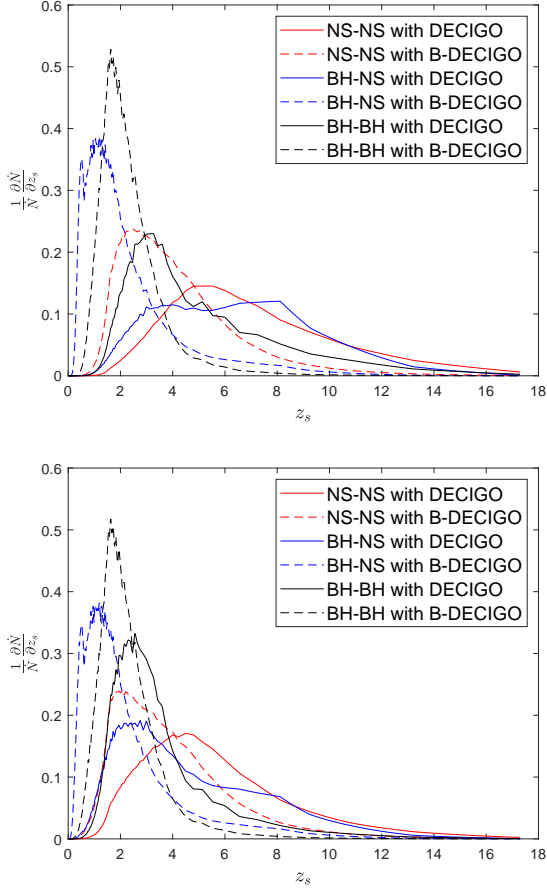


Figure 5. The normalized differential yearly detection rates $\frac{1}{N} \frac{\partial \dot{N}}{\partial z_s}$ v.s. the source redshift z_s . Upper figure corresponds to $\rho_{intr} < 8$ for the I_- image. The lower one corresponds to the I_- image including both $\rho_{intr} < 8$ and $\rho_{intr} \geq 8$. Low-end metallicity galaxy evolution and standard model of DCO formation are assumed.

Besides the magnification bias on the lensed GW events, the magnification bias at the level of the full DCO inspiral events catalogue can also be obtained. For this end, one may calculate the detection rate of the intrinsically faint events whose I_+ image is magnified above the threshold. Table 8 shows the predictions for DECIGO, and table 9 is for B-DECIGO. One can clearly see the increase in the detection rates, since $y_{+,max} > y_{-,max}$. Comparing these two tables with Tables 2 and 3, one finds out that the magnification bias at the level of the full inspiral event catalog is of the order of $10^{-3} - 10^{-4}$ depending on the DCO population. This means that the cosmological inferences drawn from this catalog would not be affected very much. One can demonstrate this effect by plotting together probability density of yearly detection rate of non-lensed sources and total prediction, which is shown in Figs. 6 and 7 for DECIGO and B-DECIGO, respectively. Figure 6 shows that the magnification bias is negligible for all three types of the DCO sources in the case of DECIGO. For B-DECIGO, the magnification bias is negligibly small for NS-NS and BH-NS binaries, while for BH-BH binaries, it is barely no-

ticeable, according to Fig. 7.

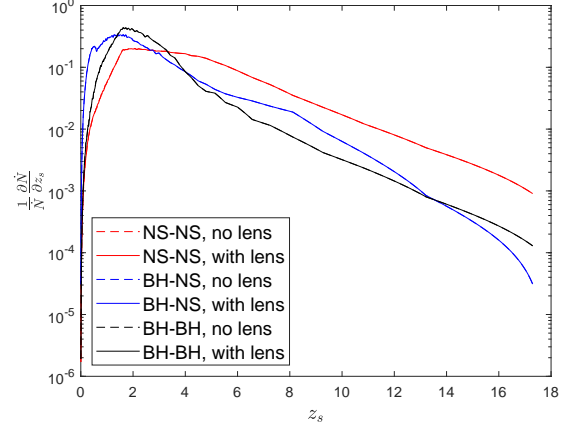


Figure 6. Probability density of DCO inspiral events yearly rate to be detected by DECIGO during its survey duty cycle $T_{surv} = 4$ years. The solid curves are for the total catalogue of lensed and non-lensed systems, and the dashed curves are for the non-lensed ones. In this particular case, the solid and the dashed curves cannot be distinguished. Note the logarithmic scale used in this figure.

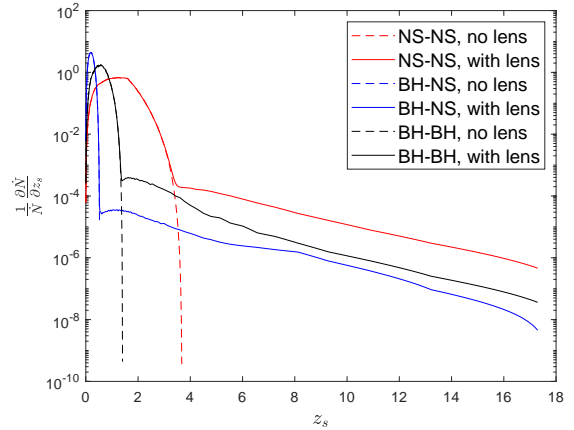


Figure 7. Probability density of DCO inspiral events yearly rate to be detected by B-DECIGO during its survey duty cycle $T_{surv} = 4$ years. The solid curves are for the total catalogue of lensed and non-lensed systems, and the dashed curves are for the non-lensed ones.

Table 8

Expected numbers of lensed GW events observed by DECIGO with $\rho_{intr} < 8$ for which the I_+ image is magnified above threshold $\rho_0 = 8$. Other assumptions and terminology – like in Table 6.

Evolutionary scenario T_{surv}	standard (4yrs;10yrs)	optimistic CE (4yrs;10yrs)	delayed SN (4yrs;10yrs)	high BH kicks (4yrs;10yrs)
NS-NS				
low-end metallicity	(17.6;19.4)	(96.7;105.5)	(17.9;18.3)	(17.6;19.5)
high-end metallicity	(15.9;17.6)	(109.3;119.3)	(16.6;18.3)	(16.2;17.9)
BH-NS				
low-end metallicity	(2.2;2.4)	(2.9;3.2)	(0.9;1.1)	(0.3;0.3)
high-end metallicity	(2.2;2.4)	(3.3;3.6)	(1.0;1.1)	(0.3;0.3)
BH-BH				
low-end metallicity	(23.6;26.3)	(43.7;48.3)	(20.6;20.8)	(2.1;2.3)
high-end metallicity	(21.5;24.0)	(44.6;49.4)	(18.7;20.8)	(1.8;2.0)
TOTAL				
low-end metallicity	(43.4;48.1)	(143.3;157.0)	(39.4;40.2)	(20.0;24.8)
high-end metallicity	(39.6;43.8)	(157.2;172.3)	(36.3;40.2)	(18.3;20.2)

Table 9

Expected numbers of lensed GW events observed by B-DECIGO with $\rho_{intr} < 8$ for which the I_+ image is magnified above threshold $\rho_0 = 8$. Other assumptions and terminology – like in Table 7.

Evolutionary scenario T_{surv}	standard (4yrs;10yrs)	optimistic CE (4yrs;10yrs)	delayed SN (4yrs;10yrs)	high BH kicks (4yrs;10yrs)
NS-NS				
low-end metallicity	(0.02;0.02)	(0.2;0.2)	(0.02;0.04)	(0.02;0.02)
high-end metallicity	(0.04;0.04)	(0.2;0.2)	(0.04;0.04)	(0.04;0.04)
BH-NS				
low-end metallicity	(0.4;0.4)	(0.9;0.9)	(0.2;0.1)	(0.04;0.04)
high-end metallicity	(0.2;0.2)	(0.7;0.7)	(0.1;0.1)	(0.03;0.03)
BH-BH				
low-end metallicity	(35.1;37.1)	(123.4;130.8)	(27.3;19.8)	(1.7;1.8)
high-end metallicity	(24.0;25.4)	(102.5;108.6)	(18.7;19.8)	(1.2;1.2)
TOTAL				
low-end metallicity	(35.5;37.5)	(124.5;131.9)	(27.5;19.9)	(1.8;1.9)
high-end metallicity	(24.2;25.6)	(103.4;109.5)	(18.8;19.9)	(1.3;1.3)

REFERENCES

- Abbott, B. P., et al. (The LIGO Scientific Collaboration and the Virgo Collaboration), 2016, PRL, 116, 061102
- Abbott, B. P., et al. (The LIGO Scientific Collaboration and the Virgo Collaboration), 2017a, PRL, 119, 161101
- Abbott, B. P., et al. (The LIGO Scientific Collaboration and Virgo Collaboration, FermiGamma-ray Burst Monitor, and INTEGRAL) 2017b, ApJL, 848, L13
- Abbott, B. P., et al. (The LIGO Scientific Collaboration and the Virgo Collaboration), 2019a, PRX, 9, 031040
- Abbott, B. P., et al. (The LIGO Scientific Collaboration and the Virgo Collaboration), 2019b, PRD, 100, 104036
- Abbott, B. P., et al. (The LIGO Scientific Collaboration and the Virgo Collaboration), 2020, ApJL, accepted [arXiv:2001.01761]
- Amaro-Seoane, P., et al. 2017, arXiv:1702.00786
- Armano, M., et al. 2016, PRL, 116, 231101
- Belczyński, K., Kalogera, V., Bulik, T. 2002, ApJ, 572, 407
- Biesiada, M., Ding, X., Piórkowska, A., Zhu, Z.-H. 2014, JCAP, 10, 080
- Cao, S., Pan, Y., Biesiada, M., Godłowski, W., & Zhu, Z.-H. 2012, JCAP, 03, 016
- Cao, S., Biesiada, M., Gavazzi, R., Piórkowska, A., & Zhu, Z.-H. 2015, ApJ, 806, 185
- Cao, S., et al. 2019, NatSR, 9, 11608
- Cao, Z., Li, L.-F., Wang, Y. 2014, PRD, 90, 062003
- Choi, Y.-Y., Park, C., & Vogeley, M. S., 2007, ApJ, 658, 884
- Collett, T. E., Bacon, D. 2017, PRL, 118, 091101
- Coulter, D. A., et al. 2017, Science, 358, 1556
- Dai, L., Venumadhav, T., Sigurdson, K. 2017, PRD, 95, 044011
- Ding, X., Biesiada, M., & Zhu, Z.-H. 2015, JCAP, 12, 006
- Dominik, M., et al. 2012, ApJ, 759, 52
- Dominik, M., et al. 2013, ApJ, 779, 72
- Fan, X.-L., Liao, K., Biesiada, M., Piórkowska-Kurpas, A., & Zhu, Z.-H. 2017, PRL, 118, 091102
- Goldstein, A., et al. 2017, ApJL, 848, L14
- Isoyama, S., Nakano, H., Nakamura T. 2018, Prog. Theor. Exp. Phys. 073E01
- Kawamura, S., et al. 2019, IJMPD, 28, 1845001
- Koopmans, L. V. E., et al. 2009, ApJL, 703, L51
- Li, S. S., Mao, S., Zhao, Y., & Lu, Y. 2018, MNRAS, 476, 2220
- Liao K., Fan X.-L., Ding X.-H., Biesiada M., Zhu Z.-H. 2017, Nat. Commun., 8, 1148
- Liao, K., Ding, X., Biesiada, M., Fan, X.-L., Zhu, Z.-H. 2018, ApJ, 867, 69
- Liao, K., Biesiada, M., & Fan, X.-L. 2019, ApJ, 875, 139
- Nakamura, T. 1998, PRL, 80, 1138
- Nakamura T., et al. 2016, Prog. Theor. Exp. Phys. 093E01 [arXiv:1607.00897]
- Ng, K. K. Y., Wong, K. W. K., Broadhurst, T., & Li, T. G. F. 2017, PRD, 97, 023012
- Oguri, M. 2018, MNRAS, 480, 3842
- Phinney, E. S. 2001, arXiv:0108028
- Piórkowska, A., Biesiada, M., Zhu, Z.-H. 2013, JCAP, 10, 022
- Sato S., et al. 2017, J. Phys.: Conf. Ser. 840, 012010
- Sereno, M., Sesana, A., Bleuler, A., Jetzer, P., Volonteri, M., & Begelman, M. C. 2010, PRL, 105, 251101
- Sereno, M., Jetzer, P., Sesana, A., & Volonteri, M. 2011, MNRAS, 415, 2773
- Seto, N., Kawamura, S., & Nakamura, T. 2001, PRL, 87, 221103

Takahashi, R. & Nakamura, T. 2003, ApJ, 595, 1039
Taylor, S. R. & Gair, J. R. 2012, PRD, 86, 023502
Wei, J.-J. & Wu, X.-F. 2017, MNRAS, 472, 2906
Yagi, K. & Seto, N. 2011, PRD, 83, 044011
Yagi, K. 2013, IJMPD, 22, 1341013

Yang, L., Ding, X., Biesiada, M., Liao, K., Zhu, Z.-H. 2019, ApJ,
874, 139
Zhu, Z.-H. & Wu, X.-P. 1997, A&A, 324, 483
Zhu, Z.-H. 1998, A&A, 338, 777